The Impact of HCl on Alkali-Induced Corrosion of Stainless Steels/FeCrAl Alloy at 600 °C: The Story After Breakaway

Citation for the original published paper (version of record):
Ssenteza, V., Jonsson, T., Nockert, J. et al (2024). The Impact of HCl on Alkali-Induced Corrosion of Stainless Steels/FeCrAl Alloy at 600 °C: The
Story After Breakaway. High Temperature Corrosion of Materials, 101(5): 1067-1076.
http://dx.doi.org/10.1007/s11085-024-10265-8

High Temperature Corrosion of Materials (2024) 101:1067–1076
https://doi.org/10.1007/s11085-024-10265-8

ORIGINAL PAPER

The Impact of HCl on Alkali-Induced Corrosion of Stainless Steels/FeCrAl Alloy at 600 °C: The Story After Breakaway

Vicent Ssenteza[1] · **Torbjörn Jonsson**[1] · **Johanna Nockert**[2] · **Jesper Liske**[1]

Received: 6 July 2024 / Revised: 6 July 2024 / Accepted: 17 July 2024 /

Abstract

The impact of Cl on alkali-induced high-temperature corrosion of stainless steels/FeCrAl alloys after breakaway oxidation was investigated in a simulated biomass- and waste-fired boiler environment at 600 °C. For this investigation, three alloys were exposed to low Cl load environment (H_2O+KCl) and to high Cl load (H_2O+KCl+HCl). Post-exposure analysis showed that the stainless steel SVM12 experiences fast oxidation and forms thick double-layered Fe-rich oxide scales. The corrosion attack is further accelerated with addition of HCl for this material with the effect being more pronounced in the inward-growing scale. The FeCrAl and FeCrNi alloys exhibit slower oxidation kinetics after the breakaway corrosion compared to SVM12 in the H_2O+KCl exposure. Furthermore, in contrast with SVM12, the addition of HCl did not accelerate the corrosion attack on these alloys. It is argued that the properties of the secondary oxide layer formed after breakaway corrosion are important in the continued corrosion resistance against chlorine-induced corrosion attack. Especially, the Cr content in the inner scales is suggested to be important in corrosion mitigation.

Keywords Oxidation · Biomass · Breakaway · Secondary protection · Chlorine

---

✉ Vicent Ssenteza
ssenteza@chalmers.se

Torbjörn Jonsson
torbjorn.jonsson@chalmers.se

Johanna Nockert
johanna.nockert@kanthal.com

Jesper Liske
jesper.liske@chalmers.se

[1] Chalmers University of Technology, Kemivägen 10, 412 96 Gothenburg, Sweden

[2] Kanthal AB, Sörkvarnsvägen 3, 734 40 Hallstahammar, Sweden

Introduction

It is well established that combustion of biomass and waste generates corrosive gases/deposits consisting of, e.g., alkali salts [1]. At 600 °C and below, this environment is known to destroy the primary protection of stainless steels (Cr_2O_3 or Cr-rich $(Cr, Fe)_2O_3$)) and FeCrAl alloys $(Cr,Al)_2O_3$), causing breakaway oxidation [2, 3]. This occurs rapidly, within hours or days, in this environment, and the alloys will thereby be dependent on the scales formed after breakaway, the so-called secondary protection. The secondary protection is characterized by formation of outward-growing Fe-rich oxide and inward-growing spinel oxides, which composition depends on the alloying elements. In recent research, the concepts of good secondary protection (referring to slow-growing scale formed after breakaway) and poor secondary protection (referring to fast-growing Fe-rich scales) have been introduced to improve the understanding of oxide scale formation after the breakaway phenomenon [4].

Most of the published literature on corrosion protection at high temperatures has focused on the integrity and lifetime of the primary oxide, coupled to the effect of alloying elements, e.g., Cr/Al [4], Si [5], Mo [6]. However, previous research shows that the mechanisms controlling oxide growth kinetics after breakaway oxidation, i.e., the secondary corrosion regime, differ from the primary corrosion regime when it comes to the role of the environment [4].

The effect of chlorine containing species on the primary corrosion regime (pre-breakaway stage) is well investigated. Alkali chlorides such as KCl, NaCl and $PbCl_2$ have been reported to breakdown the primary oxide by forming alkali-chromate, the so-called chromate formation mechanism [7]. HCl has been shown to facilitate formation of metal chlorides through an electrochemical approach which involves the formation of chloride ions at the scale–gas interface and cations at the metal–scale interface via oxidation [8]. In other work, the role of Cl on the oxidation process has been attributed to its catalytic nature, which promotes the formation of volatile metal chlorides at lower pO_2, which upon diffusion through the scale to regions of higher pO_2 are converted to respective metal oxides, the so-called active oxidation mechanism [3]. On the other hand, some investigations have reported that the environment plays little or no role on the oxide scale formation beyond breakaway oxidation [9, 10]. Instead, the oxide growth kinetics has been explained by a diffusion-controlled mechanism, which is determined by the diffusivity of different cations through the spinel [11].

However, despite the extensive research carried out to understand alkali-induced corrosion, there is limited knowledge on the impact of increased Cl load on the oxide scales formed after breakaway, i.e., on the secondary protection of stainless steels and FeCrAl alloys.

The aim of this study is to investigate the impact of an increased Cl load on the scales formed after breakaway on both good secondary protection and poor secondary protection. For this purpose, high-temperature corrosion studies were conducted of three alloys: SVM12 (martensitic stainless steel), Kanthal® APMT (FeCrAl alloy) and alloy 27Cr33Ni3Mo (austenitic stainless steel), in a laboratory environment containing H_2O, KCl and HCl at 600 °C. Characterization of oxide products was performed using scanning electron microscopy (SEM) in combination with energy-dispersive x-ray (EDX) spectroscopy.

Experimental Procedures

Materials and Sample Preparation

In this study, three alloys were investigated: SVM12 (martensitic stainless steel) supplied by Vallourec S.A, APMT (FeCrAl alloy) supplied by Kanthal AB and alloy 27Cr33Ni3Mo (austenitic stainless steel) supplied by Alleima AB. The dimensions of the samples were 20 × 10 × 2 mm, and the chemical compositions are presented in Table 1.

The samples were prepared by grinding the surfaces with 800 SiC grit paper using a Struers automatic polishing machine. The ground coupons were then cleaned using acetone, followed by ultrasonic bath and finally cleaned with ethanol.

Exposures

All exposures were performed isothermally at 600 °C for 168 h. Three environments were investigated: Exposure 1) 5% O_2 + 20% H_2O + N_2 (Bal.). Exposure 2) as in 1 + 2 mg/cm^2 KCl was pre-deposited on the samples using a spray technique. In addition, an alumina boat filled with KCl(s) was placed upstream the samples at 600 °C. A detailed description of the exposure setup can be found here [12]. Exposure 3) as in 2 + 500 ppm HCl(g). The HCl(g) was introduced into the exposure system from a gas mixture of 5% HCl–95% N_2 and was regulated using a mass flow controller. The amount of HCl(g) passing through the system was double-checked by measuring the Cl content in the collecting bottle (outlet) using ion chromatography. The samples were weighed before and after all the exposures using Sartorius™ scale with the resolution of 1 µg.

Characterization

After exposure, a thin layer of gold was sputtered on the sample surfaces and thin silicon wafer was attached using glue. The coated samples were cut and polished using a Leica EM TXP. Cross sections of the samples were obtained using a Gatan PECS II broad ion beam (BIB) milling system operated at 8 kV for 6 h. The corrosion products

Table 1 Chemical composition in wt-% of alloys used in this study

Alloy	Fe	Cr	Ni	Al	Mo	Si	Mn
SVM12	Bal	10.5	0.4		0.6	0.6	0.8
Kanthal® APMT	Bal	21		5	3	0.7	0.4
Alloy 27Cr33Ni3Mo	Bal	27	33		3	0.8	2

were analyzed using scanning electron microscopy (SEM) coupled with EDS system and operated at 10 kV for imaging and 20 kV for chemical analysis.

Results

Gravimetric Analysis, Onset of Breakaway Corrosion

The onset of breakaway oxidation was studied by exposing the alloys SVM12, APMT and alloy 27Cr33Ni3Mo to H_2O+KCl at 600 °C for 4 h. Gravimetric analysis showed that all the alloys exhibit significant mass gain corresponding to a calculated oxide scale thickness of at least 5 μm (or 0.8 mg/cm^2) for Alloy 27Cr33Ni3Mo, about 6 μm (or 0.9 mg/cm^2) for APMT and about 18 μm (or 2.9 mg/cm^2) for SVM12. The calculations of oxide thickness from mass gains assume a dense oxide corresponding to the density of Fe_2O_3. As the primary oxide scale is in the sub-micron range, all three materials have undergone breakaway corrosion already after 4 h of exposure. After 4 h (i.e., post-breakaway corrosion), the three materials showcase slightly different oxidation kinetics until the exposure time reaches 168 h. For SVM12, the mass gain increases between 4 and 168 h with 7.6 mg/cm^2, APMT with 4.1 mg/cm^2 and Alloy 27Cr33Ni3Mo with 2.6 mg/cm^2. Thus, the mass gain of SVM12 is about 3 times greater compared to Alloy 27Cr33Ni3Mo after breakaway corrosion, i.e., in the secondary corrosion regime.

Gravimetric Analysis, After Breakaway Corrosion

The impact of increased Cl load on the oxidation behavior of SVM12, APMT and 27Cr33Ni3Mo after breakaway was investigated by exposing the three materials to an environment with low Cl load, i.e., H_2O+KCl and to high Cl load, i.e., H_2O+KCl+HCl at 600 °C for 168 h. In addition, the materials were also exposed to an environment without Cl (i.e., H_2O only) for reference. Figure 1 shows the mass gain of the materials after 168 h of exposure. SVM12 exhibits the thickest oxide while APMT and alloy 27Cr33Ni3Mo show thinner oxide thicknesses in all the

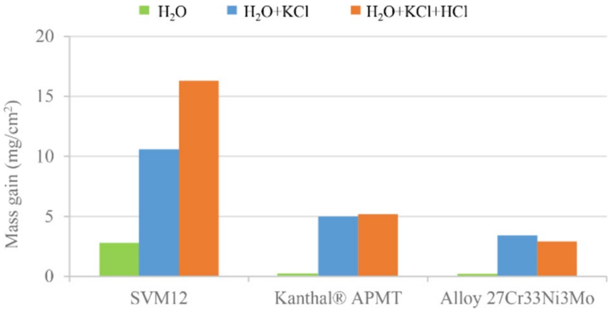

Fig. 1 Mass gain (in mg/cm^2) for SVM12, Kanthal® APMT and alloy 27Cr33Ni3Mo after 168 h exposure in H_2O, H_2O+KCl and H_2O+KCl+HCl at 600 °C

tested environments. In the absence of Cl (i.e., H_2O only), SVM12 displays an average mass gain of 2.8 mg/cm^2 which was measured to about 63 µm oxide thickness for the sample in maximum range. With addition of KCl, the mass gain increases to 10.5 mg/cm^2 (or 93 µm oxide thickness). When the Cl load is further increased through the addition of HCl, the mass gain is 16 mg/cm^2 with a measured oxide thickness of 123 µm.

The recorded mass gains and oxide thicknesses of APMT and alloy 27Cr33Ni3Mo were considerably lower in all environments. In the absence of Cl (i.e., H_2O only), APMT displays an average mass gain of 0.015 mg/cm^2 and the alloy 27Cr33Ni3Mo displays mass change of −0.01 mg/cm^2 (represented as green lines due to difference in scale). When exposed to H_2O+KCl, the mass gains of the alloys increase to 5 mg/cm^2 and 3.4 mg/cm^2 for APMT and alloy 27Cr33Ni3Mo, respectively. When exposed to H_2O+KCl+HCl, the mass gain and oxide thickness was similar compared to the corresponding exposure in H_2O+KCl.

Microstructural Investigation

Figure 2 shows SEM-BSE cross-sectional images of the SVM12 steel exposed in H_2O, H_2O+KCl and H_2O+KCl+HCl. This material forms thick and dense oxide scales in all three environments of this study (as determined from SEM analysis on BIB cross sections). The microstructural investigation shows that the scale is double layered and consists of an outward-growing and an inward-growing oxide scale. In the H_2O only exposure, SEM/EDX point analysis (marked as 1 and 2 in the images), line scans and elemental mappings show that the outer scale is composed

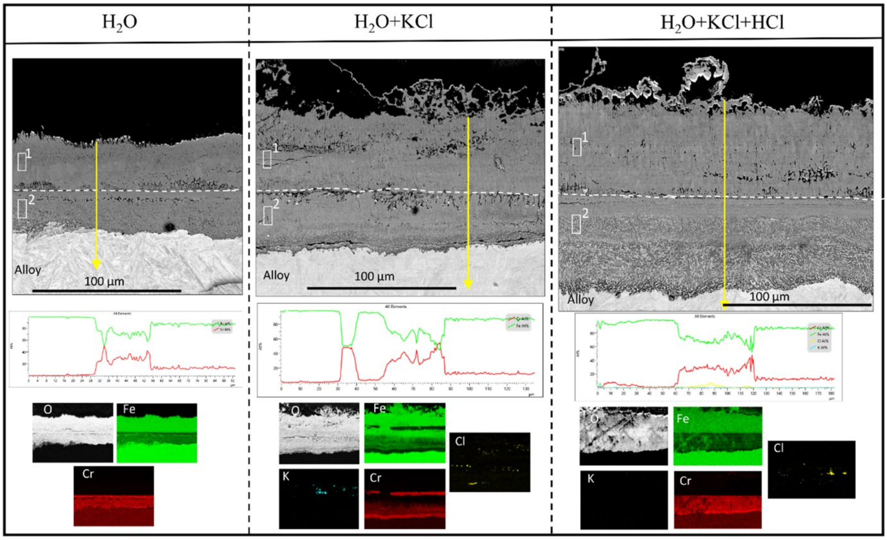

Fig. 2 SEM-BSE cross-sectional images with EDX analysis for SVM12 after 168 h exposure in H_2O, H_2O+KCl and H_2O+KCl+HCl at 600 °C

of a Fe-rich oxide while the inner scales consist of a mixed Fe,Cr oxide. In the presence of H_2O+KCl, both the outward- and inward-growing scale increase in thickness relative to the H_2O only environment. Trace amounts of K are detected in the lower part of outer layer, whereas trace amounts of Cl are detected in the outer layer as well as within the inner scale, see elemental maps.

In H_2O+KCl+HCl, the inward-growing scale of SVM12 has doubled in thickness compared to the corresponding exposure in H_2O+KCl. The outward-growing scale is only slightly thicker in H_2O+KCl+HCl exposure compared to H_2O+KCl exposure. The inward-growing scale exhibits two distinct microstructures, where the regions closer to the outer/inner scale interface are fully oxidized and dense, while the regions closer to the scale/metal interface consist of mixture of Cr-rich oxide and unoxidized metal. Trace amounts of Cl can be detected in the inner scales in both the H_2O+KCl and H_2O+KCl+HCl.

Figure 3 shows SEM-BSE cross-sectional images of a) APMT and b) alloy 27Cr33Ni3Mo. SEM/EDX analyses show that both alloys form double-layered scales consisting of Fe-rich outward-growing oxide and mixed (Fe,Cr,Al) oxide and (Fe,Cr) oxide for a) and b), respectively, in the inward-growing scales.

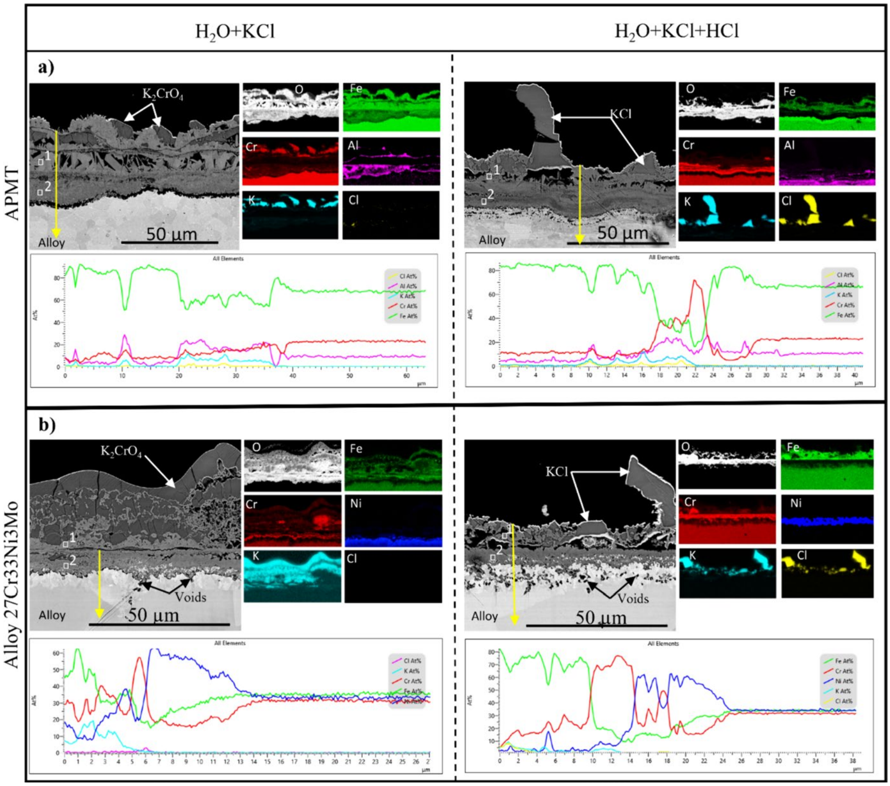

Fig. 3 SEM-BSE cross-sectional images with EDX analysis for a) Kanthal® APMT and b) alloy 27Cr33Ni3Mo after 168 h exposure in H_2O+KCl and H_2O+KCl+HCl at 600 °C

APMT forms a 34-µm-thick scale in H_2O+KCl exposure, see Fig. 3a. At the surface, large K_2CrO_4 particles embedded with Fe-rich oxide are detected. Beneath this layer, a Fe-rich scale containing large voids is detected. The composition of this oxide is 85 at-%Fe, 10 at-% Cr (cationic-%) and minor elements according to the SEM/EDX point analysis (marked as 1). The inner scale is dense and exhibits non-uniform thickness in the range of 10–18 µm. Elemental analysis (marked as 2) shows that the inner scale is composed of Fe, Cr, Al and O. In the presence of H_2O+KCl+HCl, this alloy forms a slightly thinner oxide scale compared to the corresponding H_2O+KCl exposure (~ 25 µm thick) which is well adherent to the metal. In contrast with the H_2O+KCl exposure, only KCl particles are detected at the top part of the scale, no K_2CrO_4. The inner scale is more enriched in Cr (see line scans and elemental maps) when exposed to H_2O+KCl+HCl compared to H_2O+KCl. Trace amounts of Cl in the inner scale can only be detected in the H_2O+KCl exposure and not in the H_2O+KCl+HCl exposure.

For alloy 27Cr33Ni3Mo (see Fig. 3b), the oxide scale formed in H_2O+KCl is ~ 9 µm and well adherent to the metal. At the surface, the formation of large K_2CrO_4 particles that contain cracks is prevalent, with an Fe-rich outward-growing oxide tethering the K_2CrO_4 particles. The inward-growing scale is Cr-enriched close to the metal/scale interface followed by 8-µm-deep Cr-depletion zone that is enriched in Ni. In the presence of H_2O+KCl+HCl, the oxide scale formed is ~ 9 µm thick and with large KCl particles at the surface. Similar to APMT, no K_2CrO_4 was detected on alloy 27Cr33Ni3Mo when exposed to H_2O+KCl+HCl. The outward-growing oxide is Fe-rich with the upper regions embedded in KCl particles. The inward-growing scale is composed of Cr-rich oxide mixed with oxidized metal followed by Cr-depletion zone that is enriched in Ni. Notably, an increased void concentration is observed in these Cr-depleted regions in the presence of HCl.

Discussion

The aim of this study was to investigate the impact of increased Cl load on the oxide scales formed after breakaway. Based on the results of corrosion test performed for alloys SVM12, APMT and 27Cr33Ni3Mo in low Cl load environment (H_2O+KCl) and high Cl load environment (H_2O+KCl+HCl), it is observed that all the three alloys have undergone breakaway oxidation, i.e., the slow-growing and protective corundum type oxides that normally form in mild environments have been destroyed and fast-growing iron rich scales are formed instead. Thus, the primary corrosion regime has progressed into the secondary corrosion regime during the first 4 h of exposure, which is in accordance with previous investigations done on similar alloys [4, 13]. Generally, the results show that the effect of increasing chlorine load on the secondary corrosion protection differs among the three alloys investigated. Microstructural investigation reveals that the oxide scales formed on these alloys are dense, which indicates that the scale growth is due to the diffusion of cations and anions in the scale similar to alloys exposed without Cl [4, 14]. In fact, the oxide scale morphology did not support the hypotheses of gaseous transport of chlorine through the scale, although trace amounts of Cl were detected in the scales.

SVM12 exhibits high mass gains and thick Fe-rich oxide scales under all test conditions indicating the formation of poor secondary corrosion protection. In the presence of H_2O, this material quickly undergoes breakaway oxidation, forming thick double-layered scale. This is in line with results from previous studies investigating the effect of water vapor on similar alloys [15]. The corrosion attack is increased with addition of KCl leading to fast oxidation and formation of a thicker inward-growing scale. Interestingly, the corrosion attack is further accelerated with addition of Cl in the form of HCl, with the thickness of the inward-growing scale contributing with most of the increased corrosion attack. Thus, it seems that the role of Cl in the scale growth of poor secondary protection of this material is connected to the promotion of oxygen ingress into the metal, as primarily the inward-growing part of the oxide is affected. The results indicate that the presence of Cl in the inner scale changes the diffusion properties of elements (e.g., oxygen) through the scale, which was also suggested in [16]. Attempts to better understand the exact role of chlorine in accelerating corrosion of stainless steels have been performed utilizing 3D-FIB and TEM, but it is still unclear how the presence of chlorine influences the diffusive properties [17]. Other attempts in explaining the corrosion acceleration of chlorine-induced corrosion often refer to active oxidation, where it is suggested that $Cl_2(g)$ acts as a catalyst and is transported through the oxide scales in cyclic manner via $MeCl_2(g)/Cl_2(g)$ reactions [3]. However, since the oxide scales are dense, it is questionable how a gaseous transport of $MeCl_2(g)$ and $Cl_2(g)$ could occur. Furthermore, this mechanism requires that $O_2(g)$ is disallowed to utilize the same pathways, for the chlorine cycle to work. In the present study, the results clearly show a profound oxygen ingress into the alloy upon addition of HCl, which supports the notion that Cl load further accelerates the corrosion attack on the scales with poor secondary protection.

The FeCrAl alloy (APMT) and austenitic stainless steel (alloy 27Cr33Ni3Mo) exhibit improved corrosion resistance in Cl containing environments as revealed by their slow oxidation kinetics and formation of Cr-rich inward-growing scales indicating that these alloys form, in comparison with SVM12, good secondary protection after breakaway. This improved corrosion resistance is attributed to high contents of alloying elements such as Cr, Al and Ni in the alloys (see compositions in Table 1) which enables the formation of more protective Cr-rich inward-growing scales, which is in accordance with previous works, e.g., [4]. It is noted that with addition of HCl, the oxide scale thickness is unaffected or slightly thinner. Instead, the inward-growing oxide is more enriched in Cr with the addition of HCl to the environment. The scale growth for alloys that form good secondary protection is, in addition to being diffusion controlled, associated with the formation of corrosion products. In the case of H_2O+KCl, corrosion proceeds by formation of K_2CrO_4 on the surface. The degree of corrosion resistance is dependent on constant replenishment of Cr to the surface. On the other hand, upon addition of HCl, the formation of K_2CrO_4 is hindered, and instead, the KCl is stabilized on the surface. Consequently, alloys exhibiting good secondary protection can experience Cr enrichment in the inner scales faster with addition of HCl leading to improved corrosion resistance.

Conclusion

The impact of Cl load on alkali-induced corrosion of SVM12, Kanthal® APMT and alloy 27Cr33Ni3Mo after breakaway oxidation was investigated at 600 °C for 168 h. The FeCr alloy (SVM12) exhibits poor corrosion resistance and forms fast-growing Fe-rich oxide scales that are further accelerated in high chlorine load. The more highly alloyed materials (APMT and alloy 27Cr33Ni3Mo) exhibit improved corrosion resistance in low Cl load forming Cr-rich inner scales, and the increased Cl load does not accelerate the corrosion attack on these alloys.

Acknowledgements This project has received funding from the European Union's Horizon 2020 research and innovation program under grant agreement No. 815147 (BELENUS). The study was conducted at the High Temperature Corrosion Center (HTC) at Chalmers University of Technology. Microscopy was performed at the Chalmers Materials Analysis Laboratory (CMAL).

Author Contribution V.S contributed to conceptualization, methodology, investigations, data curation, data validation, writing (original draft, review & editing). T.J contributed to conceptualization, data validation, writing (review & editing). J.N contributed to writing (review & editing). J.L contributed to conceptualization, writing (review & editing), supervision, project administration.

Funding Open access funding provided by Chalmers University of Technology.

Data availability Data will be made available on request.

Declarations

Conflict of interest The authors declare no competing interests.

References

1. W. Ma, et al., *Progress in Energy and Combustion Science* **76**, 2020 (100789).
2. T. Furugaki, H. Takahashi, and S. Hayashi, *High Temperature Corrosion of Materials* **101**, 2024 (61).
3. H. Grabke, E. Reese, and M. Spiegel, *Corrosion science* **37**, 1995 (1023).
4. A. Persdotter, et al., *Corrosion Science* **177**, 2020 (108961).
5. J. Eklund, et al., *Corrosion Science* **144**, 2018 (266).
6. R. Zhou, et al., *Materials Characterization* **204**, 2023 (113221).
7. J. Pettersson, et al., *Oxidation of Metals* **64**, 2005 (23–41).
8. N. Folkeson, L.-G. Johansson, and J.-E. Svensson, *Journal of the Electrochemical Society* **154**, 2007 (C515).
9. T. Jonsson, et al., *Oxidation of Metals* **85**, 2016 (509).
10. M. Olivas-Ogaz, et al., *Oxidation of Metals* **87**, 2017 (801).
11. T. Jonsson, et al., *Oxidation of Metals* **87**, 2017 (333).
12. V. Ssenteza, et al., *Corrosion Science* **213**, 2023 (110896).
13. N. Israelsson, et al., *Oxidation of Metals* **84**, 2015 (105).

14. T. Jonsson, et al., *Corrosion Science* **75**, 2013 (326).
15. W. J. Quadakkers and J. Żurek, in *Shreir's Corrosion*, eds. B. Cottis, M. Graham, R. Lindsay, S. Lyon, T. Richardson, D. Scantlebury, et al. (Elsevier, Oxford, 2010), pp. 407–456.
16. J. Phother-Simon, et al., *Fuel* **357**, 2024 (130012).
17. J. Phother-Simon, I. Hanif, J. Liske, and T. Jonsson, *Corrosion Science* **183**, 2021 (109315).